A Highly Active, Soluble Mutant of the Membrane-Associated (*S*)-Mandelate Dehydrogenase from *Pseudomonas putida*†

Yang Xu and Bharati Mitra*

Department of Biochemistry and Molecular Biology, School of Medicine, Wayne State University, Detroit, Michigan 48201

Received April 30, 1999; Revised Manuscript Received July 13, 1999

ABSTRACT: (*S*)-Mandelate dehydrogenase (MDH) from *Pseudomonas putida*, a member of the flavin mononucleotide-dependent α-hydroxy acid oxidase/dehydrogenase family, is a membrane-associated protein, in contrast to the more well-characterized members of this protein family including glycolate oxidase (GOX) from spinach. In a previous study [Mitra, B., et al. (1993) *Biochemistry 32*, 12959−12967], the membrane association of MDH was correlated to a 53 amino acid segment in the interior of the primary sequence by construction of a chimeric enzyme, MDH−GOX1, in which the membrane-binding segment in MDH was deleted and replaced with the corresponding 34 amino acid segment from the soluble GOX. Though MDH−GOX1 was soluble, it was an inefficient, nonspecific enzyme that involved a different transition state for the catalyzed reaction from that of the wild-type MDH. In the present study, it is shown that the membrane-binding segment in MDH is somewhat shorter, ∼39 residues long. Partial or total deletion of this segment disrupts membrane localization of MDH. This segment is not important for substrate oxidation activity. A new chimera, MDH−GOX2, was created by replacing this shorter membrane-binding segment from MDH with the corresponding 20 amino acid segment from GOX. The soluble MDH−GOX2 is very similar to the wild-type membrane-bound enzyme in its spectroscopic properties, substrate specificity, catalytic activity, kinetic mechanism, and lack of reactivity toward oxygen. Therefore, it should prove to be a highly useful model for structural studies of MDH.

The mandelate pathway, found in many strains of pseudomonads, enables these organisms to utilize mandelic acid as the sole source of carbon and energy. The pathway converts (*R*)-mandelate to benzoate by the action of the enzymes mandelate racemase, (*S*)-mandelate dehydrogenase (MDH),[1] benzoylformate decarboxylase, and benzaldehyde dehydrogenase. In some strains, a truncated pathway is observed where the racemase is missing, and MDH is the first enzyme in the pathway (*1*). MDH from *Pseudomonas putida* (ATCC 12633), the focus of our study, is a flavin mononucleotide (FMN-) dependent enzyme that catalyzes the oxidation of (*S*)-mandelate to benzoylformate:

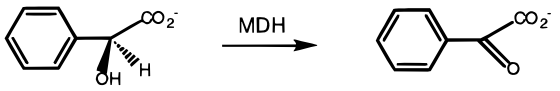

MDH belongs to a family of FMN-dependent (*S*)-α-hydroxy acid dehydrogenases and oxidases that occur in archea, bacteria, and eukarya including plants and mammals. A few of these enzymes have been studied for a number of years, including lactate monooxygenase from *Mycobacterium smegmatis*, flavocytochrome b_2 from *Saccharomyces cerevisiae*, glycolate oxidase from spinach (GOX), and long-chain α-hydroxy acid oxidase from rat kidney (*2*−*5*).

Until recently, however, the well-characterized proteins in this family were all soluble, in contrast to MDH, which is membrane-associated (*6*). Other membrane-bound proteins in this family include L-lactate dehydrogenase from *Escherichia coli*, (*S*)-mandelate and L-lactate dehydrogenases from *Acinetobacter calcoaceticus*, and L-pantoyl dehydrogenase from *Nocardia asteroides* (*7*−*9*). All the enzymes in this family oxidize an α-hydroxy acid to an α-keto acid, but the identity of the immediate oxidant depends on the particular enzyme. Oxygen is the electron acceptor for the oxidases, the flavocytochrome b_2s from yeast utilize an intramolecular heme, and the membrane-associated bacterial dehydrogenases, including MDH, most likely transfer the electron pair from the reduced flavin to a component of the electron transport chain in the membrane; the identity of the electron acceptor is not yet known. However, from the extensive sequence homology in this enzyme family as well as similarities between the three-dimensional structures of glycolate oxidase from spinach and flavocytochrome b_2 from *S. cerevisiae* (*10*, *11*), it is likely that the mechanism of the substrate oxidation partial reaction is similar for the entire family.

† This work was supported by NIH Grant GM-54102.

* Address correspondence to this author: e-mail bmitra@med.wayne.edu.

[1] Abbreviations: DCPIP, dichloroindophenol, sodium salt; GOX, glycolate oxidase from spinach; IPTG, isopropyl β-thiogalactopyranoside; LB medium, Luria−Bertani medium; KIE, substrate kinetic isotope effect; MDH, (*S*)-mandelate dehydrogenase; MDHΔ, a mutant of (*S*)-mandelate dehydrogenase with residues 177−197 deleted; MDHΔ3, a mutant of (*S*)-mandelate dehydrogenase with residues 177−215 deleted; MDH−GOX1, a chimeric mutant of (*S*)-mandelate dehydrogenase with residues 177−229 replaced by residues 176−209 of glycolate oxidase; MDH−GOX2, a chimeric mutant of (*S*)-mandelate dehydrogenase with residues 177−215 replaced by residues 176−195 of glycolate oxidase; PCR, polymerase chain reaction; PMS, phenazine methosulfate; SDS−PAGE, sodium dodecyl sulfate−polyacrylamide gel electrophoresis.

10.1021/bi990996u CCC: $18.00
Published on Web 09/03/1999

MDH is a member of an emerging subfamily of the α-hydroxy acid oxidizing enzymes, comprising of membrane-associated bacterial enzymes. In addition to MDH and lactate dehydrogenase from *E. coli* (*7*), as well as other membrane-associated FMN-dependent α-hydroxy acid dehydrogenases reported in the literature for which protein sequence data are not available (*8*, *9*), many open reading frames (ORFs) have been identified as putative members of this subfamily with the advent of genome sequencing. These include but are not limited to ORFs from *Mycobacterium tuberculosis* (J. Parkhill, Accession Number CAB06144), *Mycobacterium leprae* cosmid B38 (D. R. Smith, Accession Number L01095), *Haemophilus influenzae* (E. V. Koonin and K. E. Rudd, Accession Number P46454) and *Rhodococcus erythropolis* (R. De Mot, Accession Number AAC77479). It thus appears that membrane-associated FMN-dependent α-hydroxy acid dehydrogenases are widespread in bacteria. In an earlier work, it was shown that MDH has an internal ~50-residue insertion compared to the soluble proteins that is responsible for membrane-association (*6*). Subsequently, L-lactate dehydrogenase from *E. coli* was observed to have a similar insertion (*7*). The two proteins have 25% identity in the membrane-binding segment. The putative ORFs all have an internal insertion in the protein sequence very similar to that found in MDH, in contrast to the soluble α-hydroxy acid oxidases.

We are pursuing mechanistic and structural studies of MDH (*12*). It is difficult to solve the three-dimensional structure of MDH given the membrane-associated nature of this protein. One of our goals, therefore, was to construct a mutant of MDH that was no longer membrane-bound but retained the same substrate specificity as the wild-type enzyme and had similar catalytic efficiency. We were also interested in further exploring the exact length and structure of the membrane-anchoring segment. In an earlier study, a chimeric mutant of MDH and GOX, MDH−GOX1, was constructed that was soluble but had only 1% of the activity of the wild-type enzyme (*6*). The kinetic mechanism of the soluble mutant was different from that of the wild-type enzyme. An immediate goal, therefore, was to construct a highly active, soluble protein for three-dimensional studies.

In this work, we have constructed three structural mutants of MDH that localize in the cytosol. Characterization of the three proteins indicates that the membrane-anchoring region of MDH is confined to the internal segment that was previously suggested but is somewhat smaller. This segment is not necessary for substrate oxidation activity. Purification and detailed kinetic characterization of the three mutants identified the new chimeric mutant created in this work, MDH−GOX2, to be the most suitable candidate for future structural studies. MDH−GOX2 is highly active and preserves the same stringent substrate specificity shown by the wild-type enzyme; it appears to be slightly more efficient at oxidizing (*S*)-mandelate and small substrates than the wild-type enzyme. The kinetic mechanism for both enzymes is shown to be identical, making the soluble mutant an excellent model for the membrane-bound enzyme to investigate structural and mechanistic questions. MDH−GOX2 has recently been successfully crystallized and structural analysis is in progress.

EXPERIMENTAL PROCEDURES

Materials

Oligonucleotides were purchased from Integrated DNA Technologies, Coralville, IA. Restriction enzymes and T4 DNA ligase were obtained from either Gibco−BRL or Boehringer Mannheim Biochemicals. Vent DNA polymerase was from New England Biolabs. Geneclean Kit was from Bio101, Inc. Ni^{2+} resin was from Invitrogen or Qiagen. 2-Hydroxy acids were from Fluka or Aldrich with the following exceptions. 2-Hydroxy-3-butynoic acid was from TCI. Vinylglycolic acid and the sodium salt of indole-3-glycolic acid, as well as the [α-^{2}H] analogues, were synthesized as previously described (*12*). [α-^{2}H]-(*R*,*S*)- and (*S*)-Mandelic acids were prepared enzymatically from the protio compounds by using wild-type mandelate racemase and the H297N mutant of mandelate racemase, respectively, to catalyze the exchange of the α-proton with solvent deuterium (*13*). All other chemicals were of the highest commercial grade and were obtained from Aldrich and Sigma.

Methods

Genetic Engineering Methods: Construction of MDHΔ, MDHΔ3, and MDH−GOX2. Plasmid isolation, DNA restriction endonuclease analyses, ligations and transformations were performed as described (*14*). To facilitate purification, WT MDH is expressed in *E. coli* as a hexahistidyl-tagged protein with the histidine tag at the carboxyl terminus. The gene is under control of the *tac* promoter and is inducible by IPTG (*6*, *12*). The histidyl-tagged protein has properties identical to those of the native protein (*12*). The two deletion mutants of MDH, MDHΔ and MDHΔ3, and the chimeric mutant, MDH−GOX2, were also created as histidyl-tagged proteins.

The deletion mutant MDHΔ, with residues 177−197 deleted, was generated by overlap extension PCR with four primers (*15*). A DNA fragment encoding the amino-terminal portion of MDH (residues 1−176) was made with primers N1 and N2 and the wild-type gene as template. Similarly, a DNA fragment encoding the carboxy-terminal portion of MDH (residues 216−393 together with a hexahistidyl tag) was made with primers N3 and N4. The two DNA fragments, with a short region of overlap, were purified and mixed together with primers N1 and N3 for a final step of PCR. The resulting gene was cloned back into pKK223-3, the same expression vector as for WT MDH.

A second deletion mutant MDHΔ3, with residues 177−215 deleted, was created by a similar method, with primers N1 and N2 for the amino-terminal fragment and N3 and N5 for the carboxy-terminal fragment.

The chimeric mutant protein MDH−GOX2 was generated by deleting residues 177−215 from the MDH sequence and inserting residues 176−195 from the sequence of GOX in the corresponding position. It was also created by overlap extension PCR, with two different templates, the wild-type MDH gene as well as the gene for the first chimeric mutant MDH−GOX1, described earlier (*6*). A DNA fragment encoding the amino-terminal portion of the new chimera MDH−GOX2 was made with primers N1 and N6 and the gene for MDH−GOX1 as template. The carboxy-terminal

portion of the new chimera was made with primers N3 and N7 and the wild-type gene as template. The two DNA fragments, with a short region of overlap, were purified, mixed together, and extended/amplified with primers N1 and N3. The resulting chimeric gene was cloned into the expression vector pKK223-3.

The entire sequences of the mutant genes were confirmed by DNA sequence analysis. The sequences of the oligonucleotides used were as follows: N1, 5′-GCG-GAATTC-ATG-AGC−CAG-3′; N2, 5′-TGG-TAT-CTT-GAA-TCG-3′; N3, 5′-GCG-CTGCAG-TCA-ATG-GTG-ATG-GTG-ATG-GTG-TGC-GTG-TGT-3′; N4, 5′-CAA-GAT-ACC-AGT-GCG-ACA-CGG-C-3′; N5, 5′-TTC-AAG-ATA-CCA-TTA-GAA-ATG-CAG-GC-3′; N6, 5′-CTG-CCT-GCA-TTT-CTA-AAT-TTG-CTT-TGT-C-3′; and N7, 5′-GAT-GGA-CAA-AGC-AAA-TTT-AGA-AAT-GCA-G-3′.

Enzyme Purification. MDH, and the mutant proteins MDHΔ, MDHΔ3, and MDH−GOX2 were expressed by growing transformed cells in LB medium supplemented with 100 μg/mL ampicillin till the absorbance at 590 nm was ∼1, followed by induction with 0.5 mM IPTG for 3 h. Cells were harvested and stored at −20 °C. All purification steps were carried out at 4 °C. The purity of the proteins was judged to be >95% by SDS−PAGE.

(A) WT MDH. The purification for the carboxy-terminal histidyl-tagged MDH was modified from the protocol described earlier (*6*). The protein was solubilized from the membrane suspension with the detergent Triton X-100 and directly loaded on a 5 × 1.25 cm Ni^{2+} resin column equilibrated with buffer A (50 mM potassium phosphate, pH 7.5, 10% ethylene glycol, and 0.1% Triton X-100). The column was washed extensively with buffer A containing 50 mM imidazole. The pure protein was eluted with 400 mM imidazole in buffer A. The protein was immediately passed through a Sephadex G-25 column equilibrated in buffer A to remove imidazole and concentrated in an Amicon cell under nitrogen pressure. Finally, the buffer was made up to 20% ethylene glycol and the protein was stored in aliquots at − 70 °C.

(B) Cytosolic Mutants MDHΔ3 and MDH−GOX2. Following cell lysis by sonication in 50 mM potassium phosphate, pH 7.5, the lysate was centrifuged at 5000*g* for 10 min. The supernatant was centrifuged at 165000*g* for 90 min. The supernatant from this second centrifugation, representing the soluble component of the cell extract, contained the majority of the protein. It was made up to 10% ethylene glycol and loaded on a 5 × 1.25 cm Ni^{2+} resin column equilibrated with buffer B (50 mM potassium phosphate, pH 7.5, and 10% ethylene glycol). The column was washed extensively with 150 mM imidazole in buffer B and the protein was finally eluted with 400 mM imidazole in buffer B. The protein was immediately passed through a Sephadex G-25 column equilibrated in 20 mM potassium phosphate, pH 7.5, and 10% ethylene glycol, concentrated, and stored in aliquots at −70 °C.

(C) MDHΔ. This protein was found to localize in the soluble portion of the cell extract; however, it underwent aggregation and inactivation during purification in the absence of detergents. Hence, it was purified as described in step B, with the following modification. Following the ultracentrifugation step, 0.1% Triton X-100 was added to the supernatant. It was then purified as described in step B, with 0.1% Triton X-100 added to all the buffers.

Determination of Protein Concentration: (A) Modified Lowry. Protein concentrations were determined with the bicinchoninic acid reagent from Sigma with bovine serum albumin as standard.

(B) Flavin Content of the Protein. The protein solution was heated at 100 °C for 5 min, followed by centrifugation at 15000*g* for 5 min. The amount of released flavin was determined by measuring the absorbance at 445 nm (ϵ = 12 500 M^{-1} cm^{-1} at pH 7.5 for free FMN). The protein concentration was calculated by assuming a 1:1 molar ratio of the enzyme monomer to FMN. The two methods usually yielded values within 10% of each other.

Enzyme Assays: (A) Reduction of DCPIP or Ferricyanide. All steady-state kinetic parameters, including substrate kinetic isotope effects, were obtained by using 2,6-dichloroindophenol (DCPIP) as the electron acceptor unless specified. Activity was routinely assayed at 20 °C and in 0.1 M phosphate buffer, pH 7.5, by measuring the reduction of 100 μM DCPIP in the presence of 1 mg/mL BSA and 1 mM phenazine methosulfate (PMS) (*6*, *12*). The reaction was monitored at either 600 or 522 nm; the latter is an isobestic wavelength for the protonated and unprotonated forms of DCPIP. Potassium ferricyanide was also tested as an electron acceptor by measuring its reduction at 420 nm; in this case, PMS and BSA were omitted from the assay buffer. Extinction coefficients used for DCPIP were 21.6 mM^{-1} cm^{-1} at 600 nm and pH 7.5 and 8.6 mM^{-1} cm^{-1} at 522 nm in the pH range 4−9.5, and for ferricyanide, 1.1 mM^{-1} cm^{-1} at 420 nm.

For MDH−GOX2, we also obtained initial velocities by varying (*S*)-mandelate concentrations at different fixed nonsaturating concentrations of DCPIP, in the absence of PMS. Under these conditions, DCPIP becomes the second substrate in our assays. Data were fitted to eq 1 to generate slopes and intercepts for each line.

$$\frac{1}{V} = \frac{K_m}{V_{max}[S]} + \frac{1}{V_{max}} \quad (1)$$

The V_{max}/K_m parameter for (*S*)-mandelate was generated from the parallel line patterns that were obtained. The V_{max} and the V_{max}/K_m for DCPIP were obtained as the intercept and slope of the intercept replot.

(B) Formation of H_2O_2. The formation of H_2O_2 was measured in a coupled-enzyme assay using horseradish peroxidase and *o*-dianisidine. The assay mixture contained 0.1 M phosphate buffer, pH 7.5, 0.01 mg/mL horseradish peroxidase, 0.5 mM *o*-dianisidine, and 5−10 mM (*S*)-mandelate. Formation of the *o*-dianisidine radical cation, which reflects the oxidase activity of the enzyme, was monitored at 460 nm and at 25 °C (ϵ = 11.3 mM^{-1} cm^{-1} at 460 nm).

Determination of the Extinction Coefficient of MDH−GOX2-Bound FMN. The extinction coefficient of MDH−GOX2 at 460 nm was determined in 20 mM potassium phosphate, pH 7.5, containing 10% ethylene glycol, by comparing the absorbance of the enzyme-bound FMN with that of free FMN released on boiling the enzyme for 5 min at 100 °C.

Determination of the pK_a of Enzyme-Bound FMN. MDH−GOX2 was equilibrated in 20 mM phosphate containing 10% ethylene glycol at 4 °C. The pH was raised by small additions of a concentrated potassium hydroxide solution; in each case, the dilution was less than 0.03%. Following each addition, both the absorbance and pH were measured directly in a cuvette. The data were fitted to a modified version of the Henderson−Hasselbalch equation (*12*).

Formation of a Reversible Sulfite Adduct of FMN. Like the membrane-bound WT MDH, MDH−GOX2 also forms a reversible adduct of FMN with sulfite. The dissociation constant of the FMN−sulfite adduct was determined at 4 °C, in 20 mM phosphate buffer, pH 7.5, containing 10% ethylene glycol. MDH−GOX2 (20 μM) was incubated with different concentrations of sodium sulfite and the absorbance changes at 460 nm were measured. The data were fitted to eq 2 where the concentration of the adduct, MDH−GOX2·SO_3^{2-}, is proportional to the change in the absorbance at 460 nm of the fully oxidized MDH−GOX2 upon addition of sulfite.

$$K_d = \frac{[\text{MDH}-\text{GOX2}_{(\text{free})}][\text{SO}_3^{2-}{}_{(\text{free})}]}{[\text{MDH}-\text{GOX2}\cdot\text{SO}_3^{2-}]} \qquad (2)$$

Irreversible Inactivation by (R,S)-2-Hydroxy-3-butynoic Acid. The kinetic parameters for inactivation of MDH−GOX2 were determined in 20 mM phosphate, pH 7.5, containing 10% ethylene glycol. The enzyme (0.6 μM) was incubated with different concentrations of 2-hydroxy-3-butynoate (12−80 mM) and 150 μM DCPIP, in a total volume of 200 μL at 25 °C. At known time intervals (0−20 min), 10 μL aliquots were removed from the incubation mixture and diluted into 1.0 mL of standard assay buffer. The assays were initiated by the addition of (*S*)-mandelate. The half-time of inactivation at each concentration of 2-hydroxy-3-butynoate, $t_{1/2}$, was obtained from a semilog plot of percent remaining activity versus time. The inhibition constant K_i and the rate of inactivation, k_i, were calculated from eq 3, where [I] is the concentration of inhibitor:

$$\frac{t_{1/2}}{0.693} = \frac{1}{k_i} + \frac{K_i}{k_i[\text{I}]} \qquad (3)$$

The ratio of k_{cat} to k_i gives the turnover-to-inactivation ratio of 2-hydroxy-3-butynoate for MDH−GOX2. This ratio was also determined by a more direct method. The enzyme (0.03 μM) was incubated with ∼80 mM 2-hydroxy-3-butynoate and 150 μM DCPIP in a total volume of 0.45 mL. The decrease in absorbance at 522 nm due to the reduction of DCPIP was monitored until there was no more change due to enzyme inactivation. The turnover-to-inactivation ratio was directly calculated from the amount of DCPIP reduced during the experiment.

Instrumentation and Data Analysis. UV−visible spectra were recorded with a Cary 1E Varian spectrophotometer. Data were analyzed with KaleidaGraph for the Macintosh (Synergy Software). DNASTAR for the Macintosh (Madison, WI) was used for hydropathy analyses of MDH.

RESULTS

Membrane-Binding Domain in MDH. In an earlier work, it was shown that MDH is anchored to the membrane by an internal ∼50-residue segment, by construction of a chimeric protein of MDH and GOX (MDH−GOX1), which was no longer membrane-bound (*6*). In MDH−GOX1, residues 177−229 from MDH were deleted and replaced by residues 176−209 from the soluble GOX (boxed segment in Figure 1A). Thus, residues 177−229 in MDH were implicated in membrane binding. MDH−GOX1 had only 1% of the activity of WT MDH, implying either that MDH must be membrane-associated to be fully active or that a part of the segment exchanged in creating MDH−GOX1 (Figure 1A,B) is critical in maintaining the correct active-site structure. To create a more active and soluble mutant protein, we examined the membrane-binding segment in MDH with respect to predicted secondary structures. An examination of the crystal structure of GOX reveals that residues 198−206 form an α-helix in GOX (*16*). A structural model of MDH presented earlier, predicted that the corresponding segment, residues 218−226 in MDH, was also an α-helix (Figure 1B) (*6*). Since the α-carbon backbones in these helices from the two proteins, one soluble and the other membrane-bound, were nearly superimposable (*6*), we reasoned that the α-helix formed by residues 218−226 in MDH was not part of the membrane-binding domain. The remaining segment made up of ∼40 residues in the putative membrane-binding domain in MDH is not highly hydrophobic. Secondary structure predictions do not provide evidence of potential membrane-spanning α-helices in this region; however, an amphipathic β-strand structure is predicted for residues 177−197 (Figure 1B).

Construction of Soluble Mutants of MDH. In this study, in an attempt to create a highly active as well as soluble mutant protein, a second chimeric mutant of MDH and GOX, MDH−GOX2, was constructed. Figure 1C shows the sequence of MDH−GOX2 together with that of MDH−GOX1—these two mutant proteins are 19 residues shorter than WT MDH. In constructing MDH−GOX2, a smaller segment was exchanged compared to MDH−GOX1. Residues 177−215 were deleted from MDH and replaced by residues 176−215 from GOX. In other words, the putative α-helix formed by residues 218−226 in MDH was not exchanged with the corresponding segment from GOX. SDS−PAGE as well as the distribution of activity between the soluble and membrane-fractions indicate that MDH−GOX2 is largely soluble (Figure 2, Table 1). The extent of partitioning between the membrane and soluble fractions is quite similar for MDH−GOX2 and MDH−GOX1 (Table 1). However, in contrast to MDH−GOX1, MDH−GOX2 is highly active. Thus we can conclude that residues 216−229 in MDH, which are part of a putative α-helix, are not essential for membrane binding but appear to be critical for maintaining high levels of activity.

We next examined the importance of the predicted amphipathic β-strand in membrane association (Figure 1B). A deletion mutant was made in which residues 177−197 from MDH were deleted (Figure 1C). This mutant protein, MDHΔ, has somewhat interesting properties. It appears to localize in the soluble fraction of the cell extract according to SDS−PAGE and activity distribution (Figure 2, Table 1). However, during the purification process this protein aggregated in the absence of detergents, and it could only be purified and stored in the presence of Triton X-100. Thus, it is different from the membrane-associated WT MDH as well

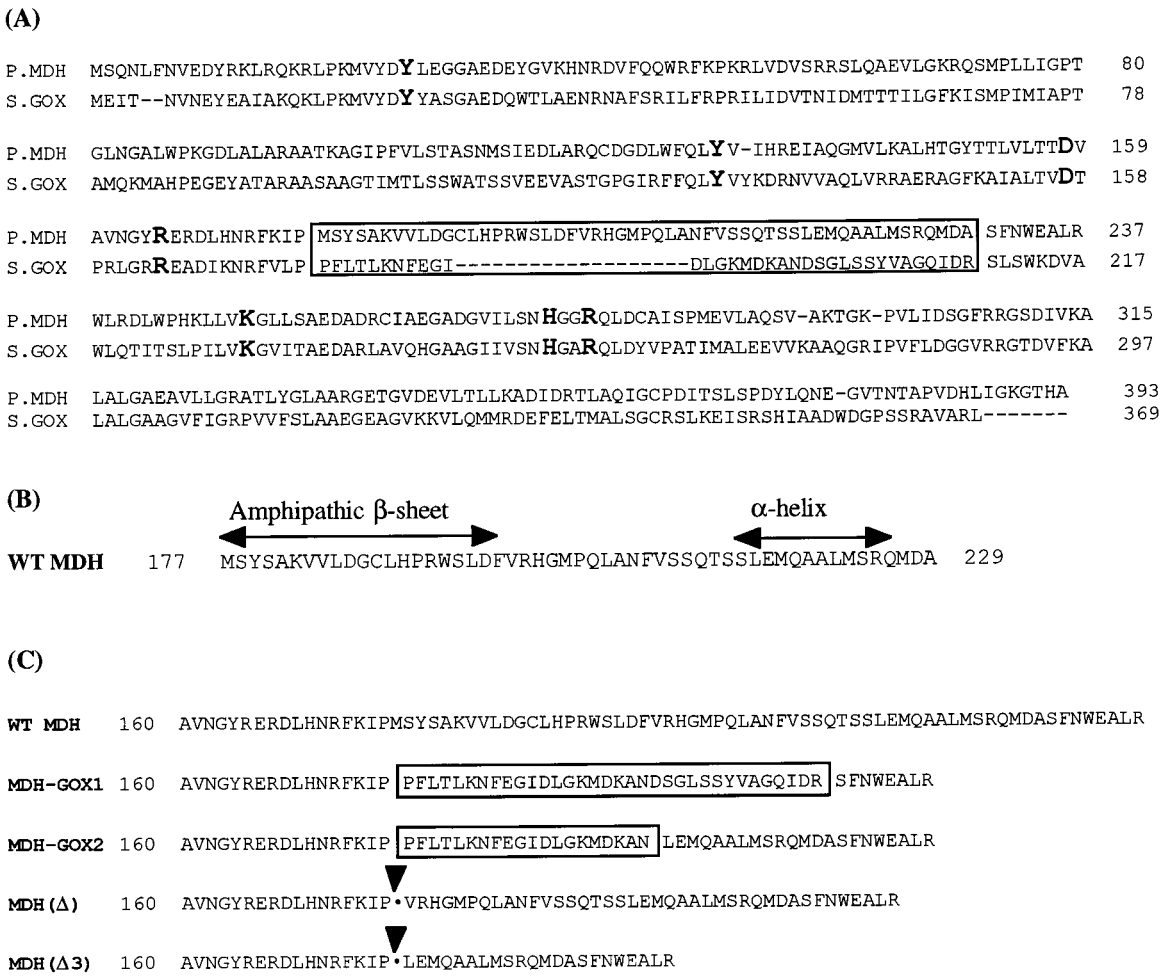

FIGURE 1: (A) Alignment of the sequences of (*S*)-mandelate dehydrogenase from *Pseudomonas putida* (P.MDH) and glycolate oxidase from spinach (S.GOX) (*19*, *20*). The residues in boldface type represent those in the active site. The boxed segments represent the internal sequences that were swapped in making the MDH−GOX1 protein (*6*). The boxed segment in MDH was originally implicated in membrane association. (B) Secondary structure predictions for the boxed internal segment of MDH depicted in (A). (C) Partial sequences of the three mutants of MDH created in this study together with those of WT MDH and the first soluble mutant, MDH−GOX1. For MDH−GOX1 and MDH−GOX2, the boxed residues represent segments from GOX that have been inserted in MDH in place of the original sequence. For MDHΔ and MDHΔ3, the arrowheads denote the positions at which residues have been deleted from the sequence of MDH.

as the cytosolic MDH−GOX1 and MDH−GOX2. It appears to be a highly active protein, with kinetic properties that are similar to those of WT MDH. Therefore, the segment deleted in creating MDHΔ, residues 177−197 in MDH, is essential for membrane association, but appears to be only part of the membrane-anchoring domain. It is not important for the substrate oxidation reaction.

Given the highly hydrophobic nature of the deletion mutant, MDHΔ, we wanted to investigate whether a segment from the soluble GOX was an absolute requirement for creating a soluble mutant of MDH, or whether we could make a fully soluble protein by deleting the entire membrane-anchoring region from MDH. Therefore we made a second deletion mutant, MDHΔ3, in which residues 177−215 were deleted from the sequence of MDH (Figure 1C). In other words, the entire segment that was exchanged in creating the active, chimeric protein, MDH−GOX2, was deleted in MDHΔ3. This mutant protein localizes in the cytosolic portion of the cell, as judged by SDS−PAGE and activity distribution (Figure 2, Table 1). Unlike MDHΔ, it does not aggregate in the absence of detergents. However, in contrast to the other two mutant proteins, MDH−GOX2 and MDHΔ, MDHΔ3 has a high K_m and low activity compared to WT MDH (Table 2). It is thus clear that the entire ∼40-residue segment (177−215) is the only membrane-anchoring region in MDH. This segment appears to be important as a spacer for maintaining the correct active-site structure; however, its composition is not important for the dehydrogenation reaction mechanism.

Enzyme Purification. All three mutant proteins, MDH−GOX2, MDHΔ, and MDHΔ3, were purified to homogeneity as carboxyl-terminus histidyl-tagged proteins. All three proteins were purified from the soluble fraction of the cell lysate. For MDHΔ, Triton X-100 was required in all the purification buffers to prevent aggregation of the protein. The proteins could be stored frozen at −70 °C in 10−20% ethylene glycol for weeks with full retention of activity. Figure 2 shows the purified MDH−GOX2; MDHΔ and MDHΔ3 were also purified to >95% homogeneity (not shown).

Enzyme Activity and Preliminary Kinetic Characterization. The rate of substrate oxidation was measured by the PMS-mediated reduction of the dye DCPIP at pH 7.5. BSA at 1 mg/mL gave the maximal activity. Table 2 summarizes the results for WT MDH, MDH−GOX1, and the three mutant proteins described in this study. The chimeric mutant,

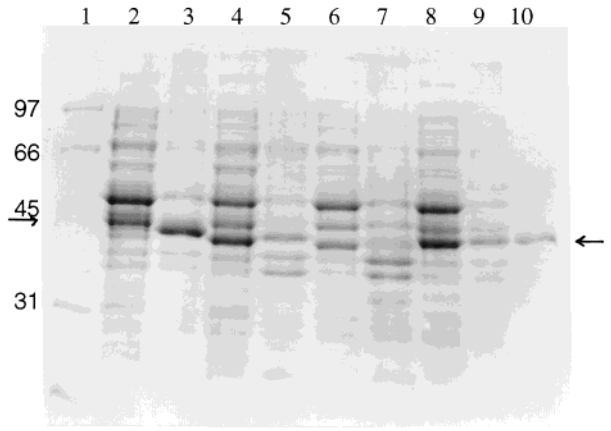

FIGURE 2: Subcellular location of MDH and its mutants analyzed by SDS−12.5% PAGE stained with Coomassie Blue. Lane 1, molecular weight markers; lanes 2 and 3, soluble and membrane fractions, respectively, of induced cells containing WT MDH; lanes 4 and 5, soluble and membrane fractions, respectively, of induced cells containing MDHΔ; lanes 6 and 7, soluble and membrane fractions, respectively, of induced cells containing MDHΔ3; lanes 8 and 9, soluble and membrane fractions, respectively, of induced cells containing MDH−GOX2; lane 10, purified MDH−GOX2. The membrane fractions are shown at a concentration that is 3-fold that of the soluble fractions, for reasons of clarity. The arrows denote the bands corresponding to MDH and the mutants. It is to be noted that the molecular weights of the proteins are in the order WT MDH > MDHΔ ∼ MDH−GOX2 > MDHΔ3.

Table 1: Distribution of MDH and Its Mutants in the Soluble and Membrane Fractions of Cell Lysates[a]

	% activity	
	supernatant	pellet
wild-type MDH	13	87
MDH−GOX1[b]	69	31
MDH−GOX2	67	33
MDHΔ	68	32
MDHΔ3	78	22

[a] After lysis, cells were centrifuged at 5000*g* for 10 min. The pellet containing cell walls, unlysed cells, and any inclusion bodies that may have been formed was discarded. The supernatant was again centrifuged at 165000*g* for 75 min. The supernatant and pellet fractions from this centrifugation were separated, and the pellet was resuspended in the same volume as the supernatant. The activities of the two fractions were determined. [b] From ref *6*.

MDH−GOX2, has a k_{cat} of 205 s^{-1} and a K_m of 85 μM. Therefore, although its activity is only ∼70% of the WT MDH value, its specificity constant, k_{cat}/K_m, is very similar to that of WT MDH for (*S*)-mandelate as substrate. In other words, it is as competent an enzyme as WT MDH in oxidizing (*S*)-mandelate. The deletion mutant, MDHΔ, with a k_{cat}/K_m that is ∼25% of that of WT MDH, is also a highly active enzyme. However, MDHΔ has a slightly higher K_m than WT MDH, indicating lower substrate affinity. The deletion mutant, MDHΔ3, in contrast, has a k_{cat}/K_m that is 1000-fold lower than that of WT MDH. This large decrease in specificity constant is partly the result of a 50-fold increase in K_m. Deletion of the entire membrane-spanning domain causes significant changes in the active site.

The substrate kinetic isotope effects (KIEs) are shown for WT MDH and all the mutants in Table 2. WT MDH has a KIE of 2.4, implying that the α-carbon−hydrogen bond-breaking step is partially rate-limiting when (*S*)-mandelate is the substrate. The same KIE is observed for MDH−GOX2 and MDHΔ, the two highly active mutant proteins, indicating that for these mutants the rate-limiting steps in the reaction are probably the same as in WT MDH. However, MDH−GOX1 and MDHΔ3, the two soluble proteins with greatly decreased activites, have KIEs that are ∼5, implying that for these proteins, the α-carbon−hydrogen bond-breaking step has become fully rate-limiting, and hence, the active site has undergone substantial changes compared to WT MDH.

WT MDH is a dehydrogenase; it does not utilize oxygen efficiently as an electron acceptor. The hydrogen peroxide formation activity was measured for the soluble mutants to investigate whether the membrane-anchoring segment played a role in suppressing reactivity toward oxygen. Table 2 shows the hydrogen peroxide formation activities obtained with WT MDH as well as the soluble mutants. All the enzymes displayed very low reactivity toward oxygen, with the highest activity of 0.1 s^{-1} obtained with the membrane-bound WT MDH.

Properties of FMN in MDH−GOX2. Figure 3 shows the absorption spectrum of purified MDH−GOX2 with absorbance maxima at 378 and 461 nm. On addition of the substrate, (*S*)-mandelate, the reduced spectrum shows a broad absorbance maximum centered at 345−350 nm. The absorbance spectrum for MDH−GOX2 is very similar to that of WT MDH (*12*). Since MDH−GOX2 does not react with oxygen at an appreciable rate, the reduced spectrum in Figure 3 could be obtained under aerobic conditions.

The extinction coefficient of MDH−GOX2 was determined to be 10 200 M^{-1} cm^{-1} at 460 nm and 20 °C, in 20 mM potassium phosphate, pH 7.5, and 10% ethylene glycol, compared to 10 400 M^{-1} cm^{-1} for WT MDH (*12*).

A pH titration of the MDH−GOX2-bound FMN revealed that just as was observed for WT MDH, the pK_a is > 10, which is close to the pK_a of free FMN in solution (data not shown) (*12*). In contrast, FMN in the soluble glycolate oxidase has a lower pK_a of 6.4 (*17*). Therefore the FMN environment in MDH−GOX2 is similar to that in WT MDH.

WT MDH forms a reversible adduct of FMN with sulfite, resulting in the disappearance of the 460 nm absorbance peak. This adduct has a dissociation constant of 30 μM at 4 °C and pH 7.5 (*12*). Titration of MDH−GOX2 with varying concentrations of sulfite showed that it also formed an FMN−sulfite adduct, with a K_d of 32 ± 1 μM (Figure 4). Thus the K_ds for the FMN−sulfite adducts are similar for WT MDH and MDH−GOX2.

Steady-State Kinetics and Isotope Effects for MDH−GOX2. WT MDH follows ping-pong kinetics with (*S*)-mandelate and the artificial electron acceptor DCPIP as the second substrate, in the absence of PMS. MDH−GOX2 displayed identical parallel line patterns in double-reciprocal plots when both (*S*)-mandelate and DCPIP concentrations were varied (data not shown). Thus, the soluble enzyme follows the same kinetic mechanism as the membrane-bound WT MDH.

Steady-state kinetic parameters were determined for MDH−GOX2 with a number of α-hydroxy acid substrates. A comparison of the data obtained for MDH−GOX2 with that of WT MDH is shown in Table 3. The k_{cat}s for (*S*)-mandelate and (*R,S*)-mandelate for MDH−GOX2 are ∼70% the values for WT MDH. The K_ms for MDH−GOX2 are correspondingly smaller. Thus, although the turnover rate

Table 2: Kinetic Parameters for WT MDH and Its Soluble Mutants, with (*S*)-Mandelate as Substrate and DCPIP as Electron Acceptor

	WT MDH	MDH−GOX1[a]	MDH−GOX2	MDH Δ	MDH Δ3
k_{cat} (s^{-1})	290 ± 12	1.6 ± 0.01	205 ± 4	150 ± 2	7.0 ± 0.1
K_m (μM)	180 ± 10	206 ± 4	85 ± 4	356 ± 16	10 000 ± 400
k_{cat}/K_m (s^{-1} M^{-1})	1.6×10^6	7.8×10^3	2.4×10^6	4.2×10^5	0.7×10^3
KIE[b]	2.4	4.6[c]	2.6	2.5	5.3
k_{cat} (H_2O_2)[d] (s^{-1})	0.10 ± 0.02	not determined	0.010 ± 0.002	0.030 ± 0.005	0.010 ± 0.003

[a] From ref *6*. [b] Substrate kinetic isotope effect using (*S*)-mandelate fully deuterated at the α-position. [c] From ref *18*. [d] Formation of H_2O_2 was assayed as described in Materials and Methods; DCPIP was not used in this assay.

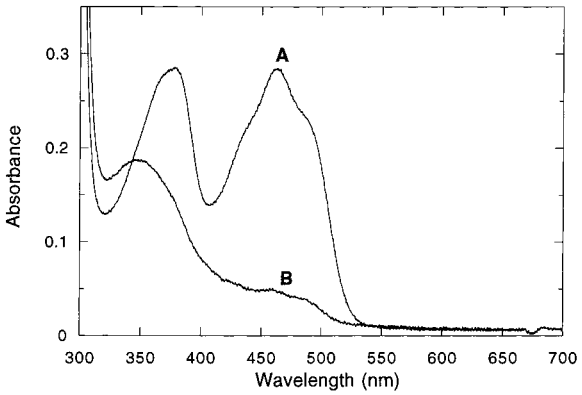

FIGURE 3: Absorbance spectra of MDH−GOX2 in the oxidized and reduced states. (A) Oxidized enzyme in 20 mM potassium phosphate, pH 7.5, and with 10% ethylene glycol; (B) after 10 mM (*S*)-mandelate was added.

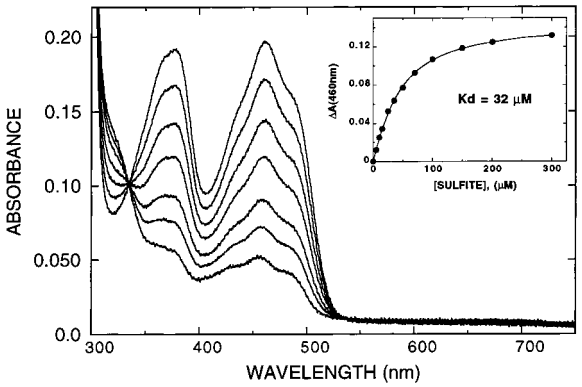

FIGURE 4: Titration of MDH−GOX2 with sodium sulfite. The enzyme was incubated with 0, 10, 25, 50, 100, and 200 μM and 5 mM sodium sulfite in 20 mM potassium phosphate, pH 7.5, and 10% ethylene glycol at 4 °C. The inset shows a plot of the FMN−sulfite adduct formed versus the total sulfite added. The solid line is a fit to eq 2.

for the soluble mutant is lower than that of the membrane-bound wild-type enzyme, the k_{cat}/K_m parameter is essentially the same for both enzymes.

In a previous study we showed that WT MDH preferentially binds substrates with bulky side chains and efficiently oxidizes only those substrates that have β-unsaturation (*12*). For example, WT MDH oxidizes mandelate and indoleglycolate at rates that are 250−2500-fold greater than for the other substrates in Table 3. The K_m decreases for substrates with bulky side chains; the K_ms for the smallest 4-carbon substrates are ∼50−100 fold higher than that for mandelate. The data obtained for MDH−GOX2 in this study confirm that the soluble mutant preserves the same stringent substrate specificity that is displayed by WT MDH. The highest k_{cat}s obtained with MDH−GOX2 are for mandelate and indole glycolate, both β-unsaturated substrates with large side chains. Saturated aliphatic hydroxy acids are poor substrates for both MDH−GOX2 and WT MDH. However, of the three aliphatic 4-carbon substrates, 2-hydroxybutyric, 2-hydroxy-3-butenic (vinylglycolic), and 2-hydroxy-3-butynoic acids, which have varying degrees of β-unsaturation, the k_{cat} increased with the degree of β-unsaturation for both MDH−GOX2 and WT MDH. Thus, 2-hydroxy-3-butynoate has the highest and 2-hydroxybutyrate has one of the lowest turnover rates of the aliphatic substrates tested in Table 2.

There is a small but notable difference between WT MDH and MDH−GOX2 as far as binding affinities for small substrates are concerned. Though MDH−GOX2 preferentially binds large substrates, it discriminates less against small substrates than does WT MDH. As shown in Table 3, the K_ms for small substrates are 2−10-fold lower for MDH−GOX2 than for WT MDH. The k_{cat}s are similar or somewhat higher for MDH−GOX2. This results in higher specificity constants (k_{cat}/K_m) obtained with MDH−GOX2 for most of the tested substrates, especially those with small side chains.

WT MDH and MDH−GOX2 show substrate kinetic isotope effects (KIEs) of 2.4 and 2.6, respectively, with (*S*)-mandelate (Table 2), suggesting that the carbon−hydrogen bond-breaking step is partly rate-limiting for both enzymes with this substrate. KIEs were also determined for (*R,S*)-indoleglycolate and (*R,S*)-2-hydroxyoctanoate. The KIEs for (*R,S*)-indoleglycolate were 3.1 and 3.6 with WT MDH and MDH−GOX2, respectively, whereas the KIEs for (*R,S*)-2-hydroxyoctanoate were 4.8 and 5.2 for WT MDH and MDH−GOX2, respectively.

Inactivation by (R,S)-2-Hydroxy-3-butynoate. 2-Hydroxy-3-butynoate is both a substrate and an irreversible inactivator for WT MDH as well as for other enzymes in the α-hydroxy acid oxidase family (*12*). The inactivation results from the formation of a covalent adduct with FMN. MDH−GOX2 was also inactivated by this acetylenic substrate with an inhibition constant, K_I, of 39.0 mM and rate of inactivation, k_i, of 0.0038 s^{-1}. Given that the k_{cat} for this substrate is 6.6 s^{-1}, the turnover-to-inactivation ratio can be calculated to be 1740. A direct measurement of the ratio of turnover to inactivation in the presence of excess 2-hydroxy-3-butynoate gives a value of 1670. The corresponding values for WT MDH are 36 mM, 0.0032 s^{-1}, and 750 for the K_I, k_i, and turnover-to-inactivation ratio, respectively (*12*). Therefore, both WT MDH and MDH−GOX2 are inhibited by 2-hydroxy-3-butynoate in a similar manner.

Activity with Different Electron Acceptors. DCPIP, ferricyanide, and oxygen were tested as electron acceptors for WT MDH and MDH−GOX2. Both WT MDH and MDH−GOX2 showed very low activities with oxygen as the electron acceptor (Table 2). For DCPIP, we obtained a K_m of ∼50 μM for both WT MDH and MDH−GOX2 from our

Table 3: Steady-State Kinetic Parameters and Substrate Kinetic Isotope Effects at pH 7.5 for WT MDH and MDH−GOX2 with Alternate Substrates[a]

	WT MDH[b]			MDH−GOX2		
	k_{cat} (s^{-1})	K_m (mM)	k_{cat}/K_m (s^{-1} mM^{-1})	k_{cat} (s^{-1})	K_m (mM)	k_{cat}/K_m (s^{-1} mM^{-1})
(*S*)-mandelate	290 ± 12	0.16 ± 0.01	1812	205 ± 4	0.09 ± 0.01	2410
mandelate	260 ± 14	0.33 ± 0.02	788	195 ± 4	0.14 ± 0.01	1390
indoleglycolate	122 ± 14	0.40 ± 0.03	305	38.5 ± 0.3	0.24 ± 0.01	160
3-phenyllactate	0.52 ± 0.01	2.0 ± 0.1	0.26	0.87 ± 0.01	1.3 ± 0.02	0.67
3-indolelactate	1.0 ± 0.01	0.9 ± 0.1	1.1	3.85 ± 0.07	0.64 ± 0.04	6.0
2-hydroxyoctanoate	0.5 ± 0.06	0.75 ± 0.1	0.67	0.96 ± 0.01	0.29 ± 0.01	3.3
2-hydroxyisocaproate	0.81 ± 0.05	4.3 ± 0.2	0.19	1.28 ± 0.01	0.49 ± 0.01	2.6
2-hydroxyhexanoate	0.34 ± 0.02	4.9 ± 0.4	0.07	0.48 ± 0.01	0.89 ± 0.04	0.54
2-hydroxyvalerate	0.36 ± 0.01	15.3 ± 1.5	0.02	0.50 ± 0.01	3.2 ± 0.1	0.16
2-hydroxyisovalerate	0.04 ± 0.00	9.5 ± 1.7	0.004	0.03 ± 0.00	2.6 ± 0.2	0.01
2-hydroxybutyrate	0.10 ± 0.01	32.0 ± 3.5	0.003	0.10 ± 0.00	13.2 ± 0.4	0.008
2-hydroxy-3-butenoate (vinylglycolate)	0.68 ± 0.03	15.4 ± 1.5	0.04	0.50 ± 0.01	10.3 ± 0.6	0.05
2-hydroxy-3-butynoate	3.9 ± 0.1	22.0 ± 1.5	0.18	6.6 ± 0.2	17.2 ± 1.1	0.38

	KIE(k_{cat}) WT MDH[b]	KIE(k_{cat}) MDH−GOX2
(*S*)-mandelate	2.4	2.6
(*R*,*S*)-indoleglycolate	3.1	3.6
(*R*,*S*)-2-hydroxyoctanoate	4.8	5.2

[a] Assay conditions are described in Materials and Methods. Unless specified, all the substrates are racemic mixtures. [b] From ref *12*.

ping-pong kinetic analyses (measured in the absence of PMS). The K_m for ferricyanide was much higher for both enzymes: values of 6.4 and 2.3 mM were obtained for WT MDH and MDH−GOX2, respectively. Similar extrapolated maximal activities were obtained with both electron acceptors for WT MDH and MDH−GOX2. Thus, DCPIP and ferricyanide were effective electron acceptors for both enzymes. However, when DCPIP alone was used, the large extinction coefficient prevented the use of saturating amounts of DCPIP. Therefore, for routine assays, PMS was used as an intermediate acceptor. PMS and ferricyanide could not be used together because of overlap of the absorbance spectra of the two compounds.

DISCUSSION

The membrane-associated FMN-dependent α-hydroxy acid dehydrogenases from bacteria are part of a large family of soluble and membrane-bound α-hydroxy acid oxidizing enzymes. There are many unanswered questions regarding the catalytic mechanisms of these enzymes, including the steps leading to substrate oxidation, the determinants of substrate specificity and the reactivity toward molecular oxygen. The three-dimensional structures of two of these enzymes have helped in the assignment of mechanistic roles to active-site residues (*16*). However, it is increasingly becoming clear that structural data for more enzymes in this family are needed to address many of the detailed mechanistic issues. Additionally, structural studies of the membrane-bound enzymes may be useful in understanding the lack of reactivity displayed by these proteins toward molecular oxygen, one of the more intriguing unresolved questions in this protein family. One of our goals is to correlate our mechanistic studies of MDH with structural information. We therefore decided to generate soluble mutants that would have the same kinetic mechanisms, substrate specificities, and catalytic rates shown by the wild-type protein, with a view to solving the structures of these soluble proteins. Another goal is to understand the role, if any, that the membrane-binding segment plays in the overall reaction.

In an earlier work it was shown that a 53-residue internal segment in MDH was responsible for membrane binding, by constructing a chimeric mutant of MDH and GOX, MDH−GOX1 (*6*). Though MDH−GOX1 was soluble, it retained only 1% of the activity of WT MDH and had lost substrate specificity. Therefore, we constructed additional mutants in this putative membrane-anchoring region to generate a more efficient enzyme. In this work, we report the construction of three soluble mutants of MDH, two of which are highly active proteins. Examination of the putative membrane-binding region and comparison with the sequence and structure of GOX revealed that an α-helical segment (residues 218−226 in MDH) that was previously believed to be part of the membrane-binding region, is actually conserved in the soluble as well as the membrane-bound enzymes in this family and may be important in preserving the correct active-site structure. The chimeric mutant, MDH−GOX2, created in this work, differs from the earlier MDH−GOX1, in that this α-helical segment in MDH is not exchanged with the corresponding residues from GOX (Figure 1). MDH−GOX2 localizes in the cytosol (Figure 2, Table 1), and is a highly active enzyme with a k_{cat}/K_m that is slightly higher than that of WT MDH. This result clearly demonstrates that the membrane-binding segment in MDH does not include this α-helical region. Additionally, the dramatic improvement in activity of MDH−GOX2 over that of MDH−GOX1 shows that this α-helix, though not directly part of the active site (*16*), is very important in maintaining the active-site structure.

We constructed two additional mutants, MDHΔ and MDHΔ3, to further investigate the length and nature of the membrane segment. Both these proteins are deletion mutants in contrast to the chimeric mutant, MDH−GOX2. In MDHΔ, a ∼20-residue segment that is predicted to be an amphipathic β-strand was deleted (Figure 1). MDHΔ has kinetic param-

eters similar to those of WT MDH (Table 2). Though this protein localizes in the cytosol, it aggregates during purification and storage in the absence of detergents. The highly hydrophobic nature of this mutant implies that the membrane-anchoring segment involves more than these deleted 21 amino acids. However, absence of this segment prevents the membrane localization of MDHΔ. Since MDHΔ proved to be a very hydrophobic protein, MDHΔ3 was constructed to investigate whether insertion of a short segment from a known soluble protein like GOX was an absolute requirement in order to produce a soluble mutant. Deletion of the entire ∼40-residue segment generates a soluble protein that does not require detergents for stability. However, MDHΔ3 is a less efficient enzyme than WT MDH. In particular, the K_m for (*S*)-mandelate is 50-fold higher in this mutant. On the basis of the properties of MDHΔ3, we can conclude that inserting a segment from GOX is not necessary to generate a soluble protein and that the ∼40-residue segment, 177−215, is the only membrane-anchoring domain in MDH. However, to generate a soluble protein in which the active-site structure is preserved, a spacer segment is necessary in place of the membrane domain.

MDH−GOX2 Is Highly Similar to WT MDH. Of the three soluble mutants, MDH−GOX2, MDHΔ, and MDHΔ3, the chimeric mutant appeared to be the most suitable candidate for future structural studies. Therefore, we investigated its properties in more detail. The absorption spectrum of the FMN cofactor in MDH−GOX2, the extinction coefficient of the enzyme-bound FMN, and its pK_a are all identical to those obtained for WT MDH (*12*). The environment of the FMN cofactor is thus unchanged in the soluble enzyme. This conclusion is reinforced by the strength of the FMN−sulfite adduct, which is also very similar to the WT MDH value (*12*). It is to be noted that WT MDH differs from other α-hydroxy acid oxidases, especially GOX, in that the values of the pK_a of the enzyme-bound FMN and the K_d of the FMN−sulfite complex are significantly higher in MDH (*17*); the properties of FMN in the soluble MDH−GOX2 are identical to those of the membrane-bound MDH and do not resemble those of the soluble GOX. In other words, the segment that was inserted from GOX does not modify the original active site of MDH to become more "GOX"-like but rather acts as a spacer to preserve the three-dimensional structure of the active site of MDH.

It was earlier shown that when (*S*)-mandelate and the artificial electron acceptor, DCPIP, are used as the two substrates in kinetic assays, MDH follows ping-pong kinetics (*12*). The soluble MDH−GOX2 was also observed to follow the same kinetic mechanism.

Substrate Specificity of MDH−GOX2. WT MDH is highly specific for α-hydroxy acid substrates with large side chains and a low pK_a of the α-proton (*12*). Steady-state kinetic data were obtained for MDH−GOX2 for substrates with varying side-chain sizes as well as highly different α-proton pK_as. When utilizing (*S*)- or (*R*,*S*)-mandelates, the soluble enzyme has a k_{cat} that is ∼ 70% of the WT MDH value. In our preparations of MDH−GOX2, 5−10% of the protein is usually in the apoprotein form, due to the loss of the noncovalent FMN cofactor. The k_{cat}s have not been corrected for this, and therefore, the soluble enzyme may have k_{cat}s that are even closer to the WT values. The K_m is half the wild-type value, indicating a 2-fold higher affinity of the soluble enzyme for the substrate. However, the specificity constants, k_{cat}/K_m, for the two enzymes are quite similar, with the soluble enzyme having a slightly higher value. Just as was observed for WT MDH, MDH−GOX2 is more specific for substrates with large side-chain sizes, with the K_ms increasing with decreasing side-chain size. More importantly, MDH−GOX2 exhibits the same high specificity toward substrates with β-unsaturation as is seen with WT MDH. Thus the soluble enzyme is identical to the wild-type enzyme in rapidly oxidizing substrates with lower pK_as of the α-proton. It is clear from Table 3 that the soluble enzyme preserves the same substrate specificity as WT MDH, and for most of the tested substrates, it is a slightly *more* efficient catalyst than the membrane-bound wild-type enzyme.

When mandelate is utilized as substrate, the carbon−hydrogen bond-breaking step is only partially rate-limiting for WT MDH as indicated by a relatively low kinetic isotope effect of 2.4. However, the carbon−hydrogen bond-breaking step becomes fully rate-limiting when substrates with higher α-proton pK_as are utilized (*12*). For both types of substrates, the FMN reductive half-reaction is fully rate-limiting, as indicated by transient kinetic studies (B. Mitra, unpublished data). These observations support a mechanism where the first step is the generation of a carbanion intermediate (*12*). An identical pattern of KIEs is seen with MDH−GOX2 (Table 3). With (*S*)-mandelate, the KIE is small (2.6); however, with 2-hydroxyoctanoate, a poor substrate, the KIE is high (5.2). Thus, MDH−GOX2 also appears to follow a mechanism involving a carbanion intermediate.

Activity with Oxygen. The identity of the physiological electron acceptor for WT MDH is not known, but it is presumably a component of the membrane electron transport chain. WT MDH does not utilize oxygen efficiently as an electron acceptor for the flavin reoxidation half-reaction; the activity is very low in oxygen-containing buffers (Table 2). To investigate the function of the membrane-binding segment in the oxidative half-reaction, the oxidase activity of MDH−GOX2 was measured. Though it is a soluble protein, MDH−GOX2 does not reduce oxygen at an appreciable rate—the hydrogen peroxide formation rate is, in fact, 10-fold lower than the WT MDH value. In contrast, the artificial electron acceptors, DCPIP as well as ferricyanide, are utilized equally efficiently by both WT MDH and MDH−GOX2. Thus, the lack of reactivity toward oxygen displayed by WT MDH is not a consequence of its membrane-binding nature. The same discrimination against oxygen is preserved in MDH−GOX2, making it a good model in future studies to investigate this issue.

Conclusions. In this work, three structural mutants of the membrane-bound MDH were constructed in order to study its membrane-anchoring domain as well as to generate a highly active and soluble protein. Our results show that a ∼40 residue segment, comprising amino acids 177−215, is required for membrane insertion. This segment is not important for substrate oxidation activity and does not play any role in the lack of reactivity to oxygen. The function of this segment may be to bring MDH in close proximity to the physiological electron acceptor in the membrane. The chimeric mutant created in this study, MDH−GOX2, was kinetically characterized. This soluble protein appears to be identical to the membrane-bound protein in terms of catalytic efficiency, substrate specificity and kinetic mechanism,

making it an ideal model for structural studies of MDH. MDH−GOX2 has been successfully crystallized recently (Y. Xu et al., manuscript in preparation) and determination of its structure is currently in progress.

ACKNOWLEDGMENT

We thank Ms. Isabelle Lehoux for providing us with the substrates, indole glycolate and vinylglycolate, as well as all the deuterated substrates used in this study.

REFERENCES

1. Fewson, C. A. (1992) in *The Evolution of Metabolic Function* (Mortlock, R. P., Ed.) pp 115−141, CRC Press, Boca Raton, FL.
2. Ghisla, S., Massey, V. (1991) in *Chemistry and Biochemistry of Flavoenzymes* (Müller, F., Ed.) Vol. II, pp 243−289, CRC Press, Boca Raton, FL.
3. Lederer, F. (1991) in *Chemistry and Biochemistry of Flavoenzymes* (Müller, F., Ed.) Vol. II, pp 153−242, CRC Press, Boca Raton, FL.
4. Stenberg, K., Clausen, T., Lindqvist, Y., Macheroux, P. (1995) *Eur. J. Biochem. 228*, 408−416.
5. Urban, P., Chirat, I., Lederer, F. (1988) *Biochemistry 27*, 7365−7371.
6. Mitra, B., Gerlt, J. A., Babbitt, P. C., Woo, C. W., Kenyon, G. L., Joseph, D., Petsko, G. A. (1993) *Biochemistry 32*, 12959−12967.
7. Dong, J. M., Taylor, J. S., Latour, D. J., Iuchi, S., Lin E. C. C (1993) *J. Bacteriol. 175*, 6671−6678.
8. Allison, N., O'Donnell, M. J., Fewson, C. A. (1985) *Biochem. J. 231*, 407−416.
9. Kataoka, M., Shimizu, S., Yamada, H. (1992) *Eur. J. Biochem. 204*, 799−806.
10. Lindqvist, Y. (1989) *J. Mol. Biol. 209*, 151−166.
11. Xia, Z., Mathews, F. S. (1990) *J. Mol. Biol. 212*, 837−863.
12. Lehoux, I. E., Mitra, B. (1999) *Biochemistry 38*, 5836−5848.
13. Landro, J. A., Kallarakal, A. T., Ransom, S. C., Gerlt, J. A., Kozarich, J. W., Neidhart, D. J., Kenyon, G. L. (1991) *Biochemistry 30*, 9274−9281.
14. Sambrook, J., Fritsch, E. F., Maniatis, T. (1989) *Molecular Cloning: A Laboratory Manual*, Cold Spring Harbor Laboratory Press, Cold Spring Harbor, NY.
15. Yon, J., Fried, M. (1989) *Nucleic Acids Res. 17*, 4895.
16. Lindqvist, Y., Branden, C.-I., Mathews, F. S., Lederer, F. (1991) *J. Biol. Chem. 266*, 3198−3207.
17. Macheroux, P., Massey, V., Thiele, D. J., Volokita, M. (1991) *Biochemistry 30*, 4612−4619.
18. Mitra, B., Gerlt, J. A., Babbitt, P. C., Kenyon, G. L., Joseph, D., Petsko, G. A. (1994) in *Flavins and Flavoproteins* (Yagi, K., Ed.) pp 621−624, Walter de Gruyter, Berlin and New York.
19. Tsou, A. Y., Ransom, S. C., Gerlt, J. A., Buechter, D. D., Babbitt, P. C., Kenyon, G. L. (1990) *Biochemistry 29*, 9856−9862.
20. Volokita, M., Somerville, C. R. (1987) *J. Biol. Chem. 262*, 15825−15828.

BI990996U